ISSN 1674-1056
http://cpb.iphy.ac.cn
http://iopscience.iop.org/cpb
中国物理 B
Chinese Physics
中国物理 Chinese Physics B

Adsorptions of metal adatoms on graphene-like BC_3 and their rich electronic properties: A first-principles study

Pengfei Sui(隋鹏飞), Jiaqi Dai(戴佳琦), Yinchang Zhao(赵银昌), Zhenhong Dai(戴振宏)

Citation: Chin. Phys. B . 2018, 27(9): 097311. **doi:** 10.1088/1674-1056/27/9/097311

Journal homepage: http://cpb.iphy.ac.cn; http://iopscience.iop.org/cpb

What follows is a list of articles you may be interested in

Quantum spin Hall insulators in chemically functionalized As (110) and Sb (110) films

Xiahong Wang(王夏烘), Ping Li(李平), Zhao Ran(冉召), Weidong Luo(罗卫东)

Chin. Phys. B . 2018, 27(8): 087305. **doi:** 10.1088/1674-1056/27/8/087305

Effect of metal catalyst on the mechanism of hydrogen spillover in three-dimensional covalent-organic frameworks

Xiu-Ying Liu(刘秀英), Jing-Xin Yu(于景新), Xiao-Dong Li(李晓东), Gui-Cheng Liu(刘桂成), Xiao-Feng Li(李晓凤), Joong-Kee Lee

Chin. Phys. B . 2017, 26(2): 027302. **doi:** 10.1088/1674-1056/26/2/027302

First-principles study of structural, electronic, and optical properties of cubic $InAs_xN_yP_{1-x-y}$ triangular quaternary alloys

I Hattabi, A Abdiche, F Soyalp, R Moussa, R Riane, K Hadji, S Bin-Omran, R Khenata

Chin. Phys. B . 2017, 26(1): 017303. **doi:** 10.1088/1674-1056/26/1/017303

Spin resonance transport properties of a single Au atom in S-Au-S junction and Au-Au-Au junction

Fangyuan Wang(王方原), Guiqin Li(李桂琴)

Chin. Phys. B . 2016, 25(7): 077304. **doi:** 10.1088/1674-1056/25/7/077304

Van der Waals heterostructure of phosphorene and hexagonal boron nitride: First-principles modeling

Peng Zhang(张鹏), Jing Wang(王静), Xiang-Mei Duan(段香梅)

Chin. Phys. B . 2016, 25(3): 037302. **doi:** 10.1088/1674-1056/25/3/037302

Adsorptions of metal adatoms on graphene-like BC_3 and their rich electronic properties: A first-principles study*

Pengfei Sui(隋鹏飞)[1], Jiaqi Dai(戴佳琦)[2], Yinchang Zhao(赵银昌)[1], and Zhenhong Dai(戴振宏)[1,†]

[1] *Department of Physics, Yantai University, Yantai* 264005, *China*
[2] *Department of Physics, Renmin University of China, Beijing* 100872, *China*

(Received 8 April 2018; revised manuscript received 23 June 2018; published online 28 August 2018)

Density functional calculations have been performed to investigate the adsorption of twenty two different kinds of metal adatoms on graphene-like BC_3. In contrast to the graphene adsorbed with adatoms, the BC_3 with adatoms shows many interesting properties. (1) The interaction between the metal adatoms and the BC_3 sheet is remarkably strong. The Li, Na, K, and Ca possess the binding energies larger than the cohesive energies of their corresponding bulk metals. (2) The Li, Na, and K adatoms form approximately ideal ionic bonds with BC_3, while the Be, Mg, and Ca adatoms form ionic bonds with BC_3 with slight hybridization of covalent bonds. The Al, Ga, In, Sn, and all transition metal adatoms form covalent bonds with BC_3. (3) For all the structures studied, there exhibit metal, half-metal, semiconducting, and spin-semiconducting behaviors. Especially, the BC_3 with Co adatom shows a quantum anomalous Hall (QAH) phase with a Chern number of -1 based on local density approximation calculations. (4) For Li, Na, K, Ca, Ga, In, Sn, Ti, V, Cr, Ni, Pd, and Pt, there exists a trend that the adatom species with lower ionization potential have lower work function. Our results indicate the potential applications of functionalization of BC_3 with metal adatoms.

Keywords: density functional theory, metal adatoms, graphene-like BC sheet, anomalous Hall conductivity

PACS: 73.22.–f, 68.43.Bc, 73.20.Hb **DOI:** 10.1088/1674-1056/27/9/097311

1. Introduction

Graphene, a two-dimensional honeycomb lattice of carbon, has stimulated a large number of research activities since its experimental realization.[1] So far, many exceptional features, such as the high strength of the lattice structure, massless Dirac fermions, the high thermal conductivity, and the half-integer Hall conductance, have been revealed for this atomically thin layer.[2–5] To modify the electronic properties of graphene, recent investigations have confirmed some chemical functionalized graphene structures like graphane,[6–10] grapheneoxide,[11–13] fluorographene,[14–18] etc. Meanwhile, the adsorption of metal atoms is also used to change electronic structures to enhance the applications of graphene. For instance, the adsorption of alkali and alkali-earth metal adatoms can dope electrons to graphene, resulting in a down-shift of the Dirac point;[19] metal-coated graphene possesses considerable hydrogen storage capacity;[20–22] lithium decorated graphene shows conventional superconductivity;[23] the graphene with 5d transition metal adatoms presents quantum anomalous Hall (QAH) effect,[24] etc. However, the binding energies (E_b) between the metal atoms and graphene are lower than the cohesive energies (E_c) of the corresponding bulk metals,[19,25,26] which implies that the clustering of the adatoms is inevitable. In order to increase E_b, it is proposed to substitute the carbon atoms in graphene with some metal atoms.[27] Nonetheless, the substitution of carbon atoms with metal atoms creates vacancies and damages the structure of graphene severely.[28]

It was reported that the boron doped carbon nanostructures could suppress the clustering of metal adatoms.[29–32] Most strikingly, at the same time of the production of graphene,[1] the BC_3 honeycomb sheet was also realized experimentally.[33,34] Different from graphene, the hexagonal BC_3 sheet is a semiconductor due to the lack of dangling bonds in it. For hydrogen storage, this two-dimensional (2D) BC_3 sheet has been predicted as one of the most promising host materials because there is no clustering of metal adatoms.[35,36] Recently, the Fermi surface nesting in the BC_3 was investigated, revealing that Li coated BC_3 can be taken as an experimentally feasible structure for exploring the nesting-driven quantum phases.[37] Furthermore, the topological superconductivity in doped BC_3 sheet was also predicted, which provides a promising route toward the realization of a genuine 2D helical p+ip superconductor.[38] Therefore, it is important to systematically investigate the adsorption of metal atoms on the BC_3 sheet. In this paper, twenty two different metal adatoms, whose adsorptions on graphene or silicene have been studied,[19,39,40] are used to study their adsorption properties on the BC_3 sheet. The binding energy, geometry, density of states (DOS), dipole moment, charge transfer, and work function of each adadatom–BC_3 structure are calculated. The calculation details are described in Section 2. The results on

*Project supported by the National Natural Science Foundation of China (Grant Nos. 11774396 and 11704322) and Shandong Natural Science Funds for Doctoral Program, China (Grant No. ZR2017BA017).

†Corresponding author. E-mail: zhdai@ytu.edu.cn

© 2018 Chinese Physical Society and IOP Publishing Ltd

structural and electronic properties of metal adatom on BC_3 are presented in Section 3. Section 4 is the summary.

2. Method

The spin-polarized density functional theory (DFT) is employed in our calculations by using the Vienna *ab initio* simulation package (VASP) code.[41] The projector augmented-wave (PAW) method[42] is adopted with an energy cutoff of 520 eV. The generalized gradient approximation (GGA) with Perdew–Burke–Ernzerhof (PBE)[43] exchange correlation energy is used. For the pristine BC_3 unit cell, in which there are two boron atoms and six carbon atoms, we use the Brillouin zone (BZ) samplings with $12 \times 12 \times 1$, $18 \times 18 \times 1$, and $36 \times 36 \times 1$ Monkhorst–Pack grids[44] for relaxations, static calculations, and density of state calculations, respectively. The Monkhorst–Pack grid for a BC_3 supercell is chosen to be inversely proportional to the dimensions of the supercell. The vacuum space along the z direction is larger than 15 Å. The tolerance for the energy convergence is 10^{-5} eV and all structures are fully relaxed until the force on each atom is smaller than 0.01 eV/Å. The dipole corrections implemented in VASP code[45,46] are applied to potentials and total energies in all systems to remove the spurious dipole interactions between the periodic images.

3. Results and discussion

The bond lengths of B–C and C–C bonds in the BC_3 sheet are 1.56 Å and 1.42 Å, respectively, which is consistent with the previous work.[47,48] The lattice constant of BC_3 unit cell is 5.17 Å which is larger than twice of that of graphene due to the existence of the B–C bonds. The electronic structure shown in Fig. 1 indicates that the energy gap of pristine BC_3 is 0.66 eV. The Dirac state is 2.4 eV above the Fermi level. The maximum valence band (VBM) locates at the Γ point while the minimum conduction band (CBM) is at M point. Figure 1 also shows the decomposed charge densities of the VB and CB at other symmetry points. In addition, the work function of the pristine BC_3 sheet is 5.52 eV while for graphene it is 4.49 eV.[19] Because the atomic radius of the boron atom is larger than that of carbon atom, this is in contradiction to the general trend that the larger the atomic radius, the smaller the work function, but consistent with the trend found in silicene.[40]

A supercell consisting of (2×2) BC_3 unit cells presented in Fig. 2 is adopted for the calculations of the adsorption of metal atoms on BC_3. The distance between the neighboring metal adatoms is 10.35 Å which is larger than 9.88 Å as considered for the 4×4 graphene supercell.[19] The K atom has the largest atomic radius among all the adatoms considered. The difference of the binding energy of the K adatom on the (2×2) and (3×3) BC_3 supercells is less than 5 meV. Thus, the interaction between the metal adatoms is so weak that the structures with a metal adatom on the (2×2) BC_3 supercell can be taken as an approximation of an isolated adatom on BC_3. We have considered six different adsorption sites as follows: the hollow site above the center of a carbon hexagon (H1), the hollow site above the center of a boron-carbon hexagon (H2), the top site above a carbon atom (T1), the top site above a boron atom (T2), the bridge site above the center of C–C bond (B1), and the bridge site above the center of B–C bond (B2), as shown in Fig. 2. The binding energy of metal adatoms on BC_3 is defined as $E_b(M) = E(M) + E(BC_3) - E(M\text{–}BC_3)$, where $E(M)$, $E(BC_3)$, and $E(M\text{–}BC_3)$ are the energies of an isolated metal atom, the BC_3 supercell, and the adatom–BC_3 system, respectively. The larger values of E_b represents the stronger binding of the metal adatom to BC_3 sheet.

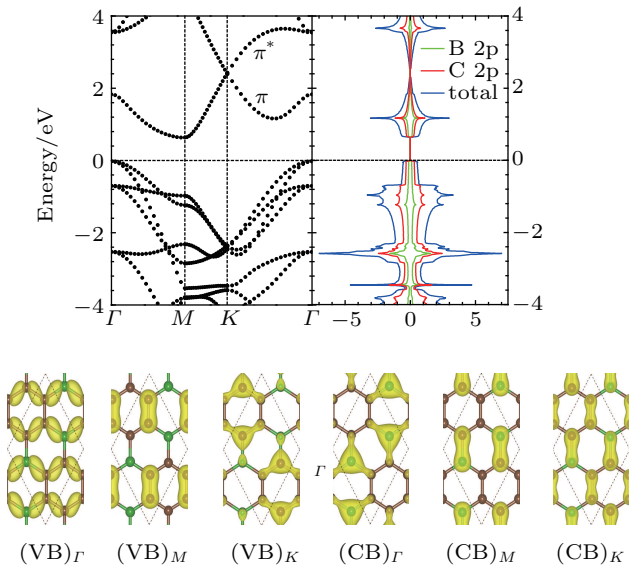


Fig. 1. (color online) The band structure, projected density of states (PDOS), and band decomposed charge densities of VB and CB at the Γ, M, and K symmetry points for pristine BC_3 unit cell. The Fermi level is set to be at zero.

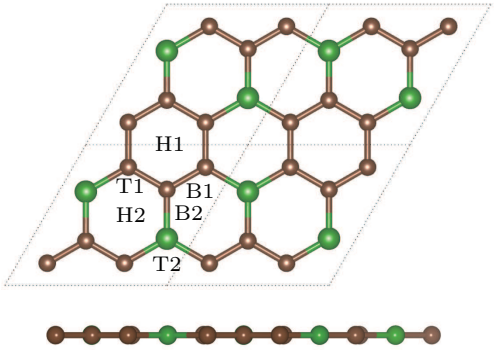


Fig. 2. (color online) Top view and lateral view of the (2×2) structure of the hexagonal BC_3. The big and the small balls represent the boron and carbon atoms, respectively. Six different adsorption-sites are labeled as H1, H2, T1, T2, B1, and B2.

3.1. Energetic, structural, and electronic properties

For each adatom, the adsorption on the six possible sites are investigated firstly, as shown in Fig. 3. Possible diffusion pathways and the energy barrier of the adatoms on BC_3 lattice can be deduced from the binding energy on each site. For example, the diffusion pathway of Li from H1 to H2 sites is H1→B1→H2 and the corresponding energy barrier is 0.41 eV, while the diffusion path between the adjacent H2 sites is H2→B2→H2 with an energy barrier of 0.38 eV. The exact diffusion energy barrier can be calculated using the nudged elastic band (NEB) method.[49] They are about 0.42 eV and 0.39 eV for the above two pathways, which are close to the difference between the E_b's at the corresponding adsorption sites. In addition, the energy barrier from H2 to H1 is 0.32 eV.

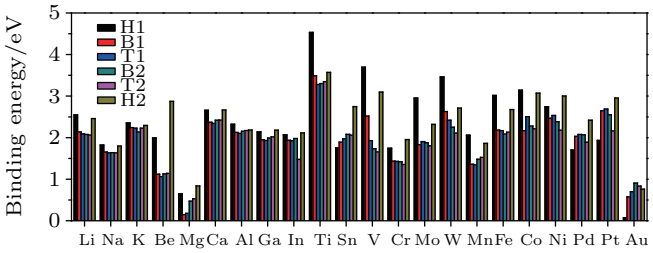


Fig. 3. (color online) Binding energy of 22 different metal adatoms on six possible adsorption sites of the (2×2) BC_3 sheet. The data on sites of H1, B1, T1, B2, T2, and H2 are listed from left to right for each adatom studied.

Therefore, Li adatoms on the BC_3 sheet favor the diffusion path H1→B1→H2→B1→H1 with the largest barrier value of 0.42 eV. Upon full geometry optimization, Li, Na, K, Al, Ti, V, Mo, W, Mn, Fe, and Co favor bondings on the H1 site, while Be, Mg, Ca, Ga, In, Sn, Cr, Ni, Pd, and Pt prefer to adsorb at the H2 site. Exceptionally, Au adatoms prefer adsorbing at the B2 site of BC_3.

3.1.1. Alkali and alkali-earth metal adatoms

For Li, Na, K, and Ca, the binding energy E_b on any adsorption site is larger than the cohesive energy E_c per atom of the corresponding bulk metal, as shown in Fig. 3 and Table 1. The K adatom on BC_3 has the largest ratio of E_b to E_c ($E_b/E_c \approx 2.52$) at H1 site, and the corresponding binding energy E_b is about 2.50 eV, which is much larger than 0.86 eV and 2.04 eV of K adatoms on graphene and silicene.[19,39] Mg has the smallest E_b of 0.84 eV among all the adatoms studied. The adatom height h increases with the increase of the atomic radius of adatoms. This interprets the lowest h of Be adatom on BC_3 because Be atom has the smallest atomic radius among all the adatoms considered. Moreover, the adsorption-induced distortion of the plane of BC_3 is very small for all the alkali and alkaline-earth metal atoms.

Table 1. Properties of the metal atom adsorption on the BC_3 sheet. FS represents the favorite sites of adatoms on the BC_3, h is the adatom height defined as the difference between the adatom z coordinate and the average z coordinate of atoms in BC_3, Δ is the adsorption-induced distortion deviating from the plane of BC_3, ρ_{ad} is the charge transfer from adatom to BC_3, IP is the experimental ionization potential of the isolated atom, μ_{iso} and μ_{tot} are the magnetic moment of the isolated atom and the total magnetic moment of the system, p and Φ are the dipole moment and the work function, and E_{gap} is the energy gap of the system. The "m" and "h" in E_{gap} column represent metal and half-metal, respectively.

	FS	h/Å	Δ/Å	E_b/eV	$E_c^{(a)}$/eV	E_b/E_c	p/D	Φ/eV	ρ_{ad}/e	IP$^{(b)}$/eV	μ_{iso}/μ_B	μ_{tot}/μ_B	E_{gap}/eV
Li	H1	1.67	0.021	2.55	1.630	1.56	3.05	4.90	0.81	5.39	1.00	0.00	m
Na	H1	2.12	0.046	1.82	1.113	1.64	4.93	4.92	0.76	5.14	1.00	0.00	m
K	H1	2.50	0.071	2.35	0.934	2.52	6.19	4.94	0.81	4.34	1.00	0.00	m
Be	H2	0.94	0.080	2.87	3.320	0.86	1.50	5.15	1.54	9.32	0.00	0.00	m
Mg	H2	1.84	0.057	0.84	1.510	0.56	2.64	5.14	0.89	7.65	0.00	0.95	m
Ca	H2	1.90	0.132	2.67	1.840	1.45	6.64	5.10	1.30	6.11	0.00	0.00	m
Al	H1	2.08	0.014	2.32	3.390	0.68	0.71	4.91	0.71	5.99	1.00	0.00	m
Ga	H2	2.10	0.013	2.18	2.810	0.78	1.33	5.15	0.51	6.00	1.00	0.00	m
In	H2	2.35	0.019	2.11	2.520	0.84	2.02	5.07	0.58	5.79	1.00	0.02	m
Sn	H2	1.99	0.015	2.75	3.140	0.88	2.01	5.29	0.71	7.34	2.00	0.00	0.23
Ti	H1	1.32	0.208	4.53	4.850	0.93	4.29	5.40	1.32	6.83	3.00	0.00	0.41
V	H1	1.30	0.251	3.70	5.310	0.70	3.08	5.22	1.08	6.75	5.00	1.00	0.36
Cr	H2	1.61	0.125	1.95	4.100	0.48	3.30	5.11	0.91	6.77	6.00	4.00	m
Mo	H1	1.31	0.306	2.95	6.820	0.43	2.71	4.93	0.88	7.09	6.00	0.00	h
W	H1	1.27	0.293	3.46	8.900	0.39	2.37	4.84	0.89	7.86	6.00	0.00	0.02
Mn	H1	1.44	0.110	2.06	2.920	0.71	2.26	4.90	0.84	7.43	5.00	0.76	h
Fe	H1	1.35	0.158	3.01	4.280	0.70	1.94	4.96	0.83	7.90	4.00	2.05	m
Co	H1	1.33	0.155	3.14	4.390	0.72	1.64	4.83	0.73	7.88	3.00	1.02	m
Ni	H2	1.36	0.180	3.00	4.440	0.68	1.71	5.31	0.46	7.64	2.00	0.00	0.39
Pd	H2	1.72	0.107	2.42	3.890	0.62	1.68	5.59	0.24	8.34	0.00	0.00	0.57
Pt	H2	1.65	0.125	2.95	5.840	0.51	1.40	5.54	0.20	8.96	2.00	0.00	0.43
Au	B2	2.31	0.179	0.90	3.810	0.24	0.89	5.35	0.20	9.23	1.00	1.00	0.03

[a] From Ref. [50], [b] from Ref. [51].

Figure 4(a) shows the DOS of B 2p, C 2p, and K 4s states of K adatoms at the H1 site of BC_3. In comparison with the pristine BC_3, the electronic states of BC_3 remain almost unaltered except for the charge transfer from the adatom to the substrate. Thus the Fermi level E_F is up-shifted, resulting in metal features of the K–BC_3 structure. The 4s states of the K adatoms are empty and lie at 1.71 eV above E_F. Thus there is about one electron charge (e) per adatom transferred from the alkali metal adatoms to the BC_3 sheet. This effect has been tested by the Bader charge transfer from metal adatoms to BC_3 listed in Table 1. For Li and Na adatoms on BC_3, similar results are obtained. So the bonding of Li, Na, and K with BC_3 is ionic. Meanwhile these structures have no magnetic moment. As a result, the effect of alkali metal adsorption on BC_3 can be taken as the electron doping process only. In contrast, the Na and K adatoms on graphene are magnetic, with the spin-up s states of the adatoms lying close to E_F.[19] For the pristine BC_3 sheet there is a van Hove singularity at 1.71 eV above E_F. Increasing the coverage capacity of alkali metal atoms on BC_3, the van Hove singularity can be tuned to locate exactly at E_F, which results in the formation of Fermi surface nesting.[37] In addition, the dependence of the dipole moments on adatom height h and the amount of charge transfer can be easily observed here. For example, the Ca–BC_3 system exhibits the largest dipole moment of 6.64 debye in all cases investigated due to the relative high h (1.90 Å) and considerable charge transfer (1.30 e).

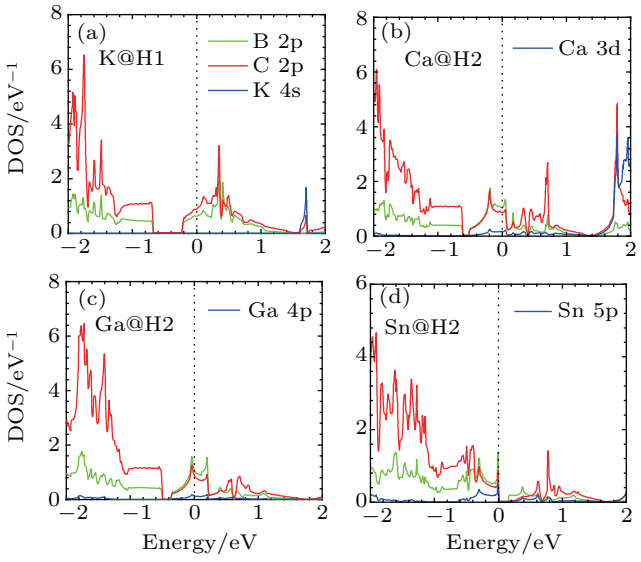


Fig. 4. (color online) PDOS for (a) K–BC_3, (b) Ca–BC_3, (c) Ga–BC_3, and (d) Sn–BC_3.

For the adsorption of Be, Mg, and Ca atoms on BC_3, slight hybridization states occur close to E_F as shown in Fig. 4(b). Figure 4(b) shows that the hybridizations between Ca 3d states and B 2p and C 2p states of BC_3 appear around E_F, which results in a partial covalent bond between Ca and the BC_3 sheet. In the case of Mg adsorbing on BC_3, the spin-up Mg 3p states hybridize with the substrate states around E_F, contrasting with the spin-down Mg 3p states hybridizing with the substrate states far above E_F. These electronic states result in the magnetism of the Mg–BC_3 structure with a total magnetic moment of 0.95 μ_B. There are also large electron transfer from alkaline-earth metal adatoms to the BC_3 sheet. For Be, Mg, and Ca the Bader electron transfers from adatoms to BC_3 are 1.54 e, 0.89 e, and 1.30 e, respectively, revealing ionic and covalent mixed binding between the adatoms and the substrate.

3.1.2. Groups III and IV metal adatoms

The E_b of Al, Ga, and In on the BC_3 sheet are almost three times as large as on graphene. Furthermore, the E_b of Sn adatom on BC_3 is 2.75 eV with the ratio E_b/E_c of 0.88, which is an order of magnitude larger than that on graphene.[19] Due to the similar atomic radii of Al, Ga, In, and Sn, the adatom heights h of the four adatoms vary from 2.00 Å to 2.35 Å, and their dipole moments vary from 0.71 debye to 2.01 debye. The charge transfer from Al, Ga, In, and Sn adatoms to the substrate are 0.71 e, 0.51 e, 0.58 e, and 0.71 e, respectively, which are much less than the corresponding values of the valence electrons. There are remarkable hybridizations between the adatom p states and the substrate states around and below E_F for Al, Ga, and In on BC_3. Figure 4(c) shows the hybridizations between the Ga 4p states and the BC_3 states around E_F. For the adsorption of Sn adatom on BC_3, similar hybridization features are observed, as shown in Fig. 4(d). Thus the bonding is mainly covalent for these adatoms on the BC_3 sheet, instead of an ionic bonding between these adatoms and graphene.[19] In addition, for the Sn adatom on BC_3, the Sn–BC_3 structure seems to be a semiconductor with an energy gap (E_g) of 0.23 eV.

3.1.3. Transition and noble metal adatoms

For the adsorption of the transition and noble metal atoms on the BC_3 sheet, the adatoms are strongly bounded to the H1 or H2 sites except for Au, which prefers to bond with the substrate at the B2 site. Among these transition metal adatoms, the E_b of Ti adatom is close to E_c, such that the ratio E_b/E_c is 0.93. The adatom d states are strongly hybridized with the B 2p and C 2p states of BC_3 around E_F for all these adatoms except Au, whose 6s states are hybridized with the substrate states near E_F, as shown in Fig. 5. Thus, the transition metal adatoms form strong covalent bonds with their nearest substrate atoms.

In details, figure 5(a) shows that for V–BC_3 the occupation of the spin-up V 3d states is much larger than that of the spin-down V 3d states, which results in a total magnetic moment of 1.00 μ_B. For Cr, Mo, and W adatoms, in spite of the large E_b (3.46 eV) of W on BC_3, the ratio E_b/E_c of them is less than 0.50. In addition, Mo adatom adsorption induces a distortion of 0.306 Å, which is the largest distortion in all the cases considered. Furthermore, the hybridizations between the adatoms d states and the BC_3 states occur through almost the entire energy space, as shown in Fig. 5(b). For Mn, Fe, Co, and Ni, adatoms and substrate are relatively strongly bonded. Co adatom on the H1 site has the largest ratio E_b/E_c of 0.72. These adatoms prefer to adsorb on the H1 sites except Ni, which favors to reside at the H2 site. The adatom–BC_3 structures are all magnetic. Figures 5(c) and 5(d) show that there are hybridizations between the adatoms and substrate around and below E_F. For Pd, Pt, and Au, the electron transfers from the adatom to the substrate are smaller compared to their valence electrons. Thus, all the adatom–BC_3 structures are semiconductors. Pd 4d (Pt 5d) states are hybridized with the B 2p and C 2p states of BC_3 nearly throughout entire energy space, as shown in Fig. 5(e). For Au adatom, the E_b is 0.90 eV which is an order of magnitude larger than that on graphene,[19] and the magnetic moment of the Au–BC_3 structure is 1.00 μ_B. Although the 5d shell of an isolated Au atom is fully filled, the Au 5d states are hybridized strongly with the substrate states below E_F, in contrast to the hybridizations between the Au 6s states and substrate states occurring near E_F, as shown in Fig. 5(f).

More interesting are the cases of Co, Mo, Mn, and Au adatoms on BC_3. In Co–BC_3 structure, there exists a single spin Dirac cone around E_F, as shown in Figs. 6(a)–6(c). LDA calculation shows that the spin-down Dirac point exactly locates at E_F with total magnetic moment of 1.00 μ_B. If the spin orbit coupling (SOC) interactions are taken into account, there is a 37 meV gap opening at the Dirac point, as shown in Fig. 6(c). This indicates that the metal atom adsorption increases the SOC interaction remarkably, and the Co–BC_3 structure may be a quantum anomalous Hall (QAH) insulator,[52,53] which will be discussed later. For Mo and Mn adatom on BC_3, the adatom–BC_3 structures are half-metals with only single spin bands across E_F, as shown in Figs. 6(d) and 6(e). For the adsorption of Au atom on the B2 site, the Au–BC_3 system is a spin-semiconductor with a small intrinsic energy gap of 30 meV, and the bandwidths of the spin-up and spin-down states near E_F are 0.18 eV and 0.30 eV, respectively, as shown in Fig. 6(f). These results imply great significance in spintronics.[54–56]

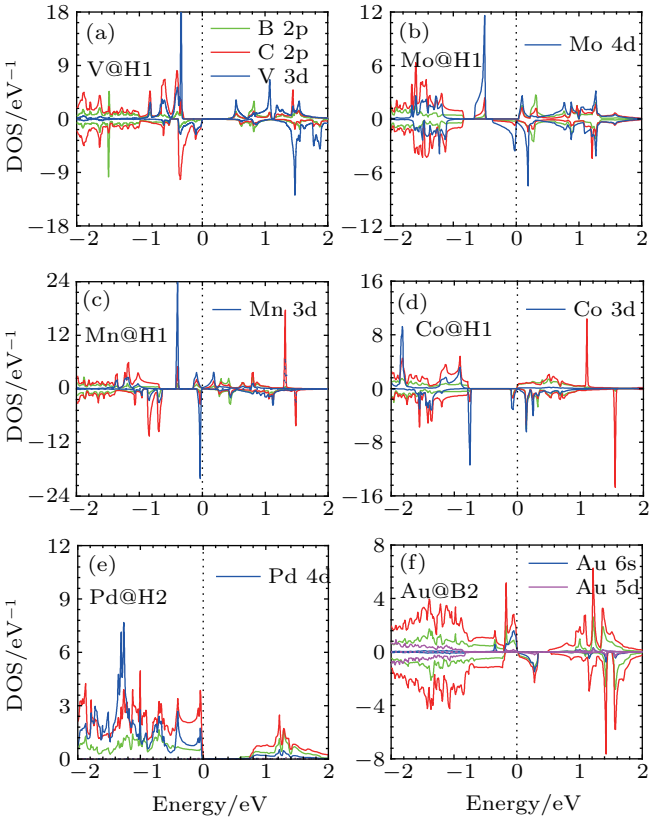


Fig. 5. (color online) PDOS for (a) V–BC_3, (b) Mo–BC_3, (c) Mn–BC_3, (d) Co–BC_3, (e) Pd–BC_3, and (f) Au–BC_3.

For the Co–BC_3 system, the ground state estimated from the LDA calculations is found to be ferromagnetic, which is about 211 meV and 45 meV lower than the nonmagnetic and antiferromagnetic states, respectively. To identify the topological property of the SOC induced insulating state, we also calculate the Berry curvature $\Omega(\boldsymbol{k})$ and Chern number for the Co–BC_3 system.[57–59] The distribution of the Berry curvature $\Omega(\boldsymbol{k})$ (in atomic units a.u.) for the whole valence bands in the momentum space is shown in the top panel in Fig. 7, in which the nonzero $\Omega(\boldsymbol{k})$ is localized around the K and K' points with the same sign. By integrating the $\Omega(\boldsymbol{k})$ over the first Brillouin zone, the anomalous Hall conductivity σ_{xy} as a function of the energy around the Fermi level is obtained, as shown in the bottom panel in Fig. 7. We can find that the quantized Hall conductance platform appears around the Fermi level and the width of the platform accords completely with the global band gap. The σ_{xy} of $-e^2/h$ means the Chern number of -1, which indicates that the Co–BC_3 structure is topologically nontrivial and thus the two chiral edge channels will appear on each side of its sample, hinting the realization of the QAH effect. In addition, the magnetocrystalline anisotropy calculation shows that the energy of the out-of-plane spin orientation for the Co–BC_3 system is about 0.2 meV lower than that of the in-plane spin orientation, implying that the Co–BC_3 is a suitable system to observe the QAH state in experiment.

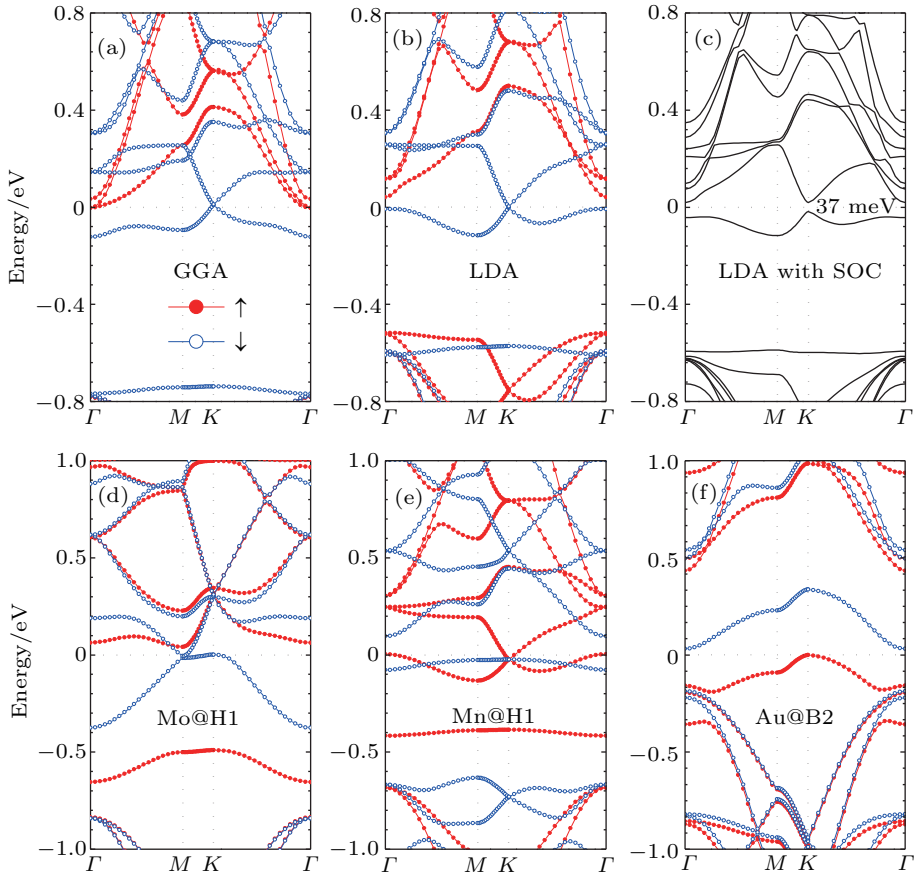


Fig. 6. (color online) Band structures for Co at the H1 site of the BC_3 calculated with the (a) GGA, (b) LDA, and (c) LDA with SOC. (d), (e), and (f) show band structures for Mo–BC_3, Mn–BC_3, and Au–BC_3, respectively.

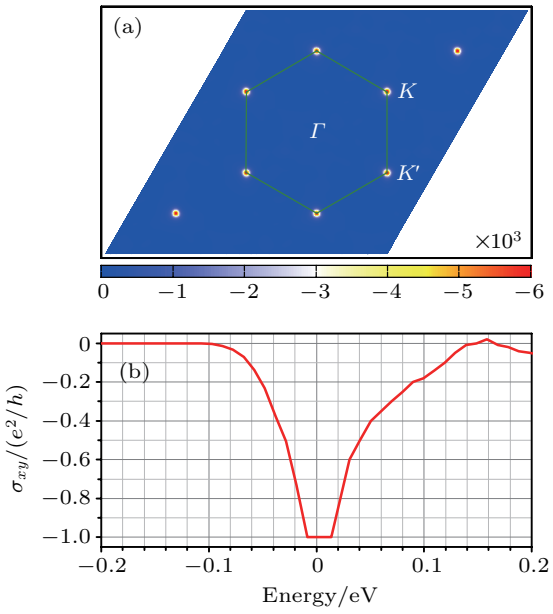


Fig. 7. (color online) (a) The distribution of the Berry curvature (in a.u.) for the whole valence bands in momentum space and (b) the anomalous Hall conductivity σ_{xy} around the Fermi level calculated from the LDA.

3.2. Relation of dipole moments vs. work functions

The dipole moment perpendicular to the substrate is determined by the real-space-charge rearrangement due to the interaction between the adatom and substrate. It is defined as[19] $p = -\int \rho(z)z\mathrm{d}z + \sum_i Z_i e z_i$, where $\rho(z)$ is the electron density integrated over the xy-plane, i is the index of ion, Z_i is the atomic number of ion, and z_i is the z coordinate of ion. The work function, which denotes the energy to remove an electron from the adatom–substrate system, can be calculated as $\Phi = E_{\mathrm{vac}} - E_{\mathrm{F}}$, where E_{vac} is the reference vacuum energy which is determined from the electrostatic potential in the vacuum region. Thus the work function is sensitive to the charge transfer from adsorbate to substrate.

To reveal the correlations between the dipole moment p and the work function Φ, we have drawn the p–Φ plot in Fig. 8(a). Except for Pd and Pt adatoms on BC_3, the work functions for all the adatom–BC_3 structures are lower than the value for the bare BC_3 sheet. The data for alkali or alkaline-earth metal atoms are linear, as shown by the gray line segments. The p–Φ trend for alkali metal adatoms on BC_3 is consistent with the data of the adatom height h and the charge transfer, due to the dipole moments are sensitive to the adatom heights h and charge transfers. For Li, Na, and K, the adatom heights h vary from 1.67 Å to 2.50 Å, while the amount of electrons transferred from the adatoms to the substrate is nearly identical, resulting in the increased dipole moments and almost unaltered work functions. It can also be seen that the

multivalent adatoms do not follow a particular trend. Figure 8(b) shows that Φ is correlated to the experimental ionization potential (IP) for an isolated atom.[51] IP represents the energy requiring to remove an electron from an isolated atom. The overall trend of IP–Φ plot is different from the plot drawn for adatoms on graphene.[19] Most of the points locate below the gray line. However, the IP–Φ plot for Li, Na, K, Ca, Ga, In, Sn, Ti, V, Cr, Ni, Pd, and Pt adatoms on BC_3 is similar to that for adatom–graphene, which shows the trend that the adatom species with lower IP are more likely to transfer their outer-shell electrons to the substrate, thereby raising E_F and lowering Φ. For other adatoms there is no such particular trend found.

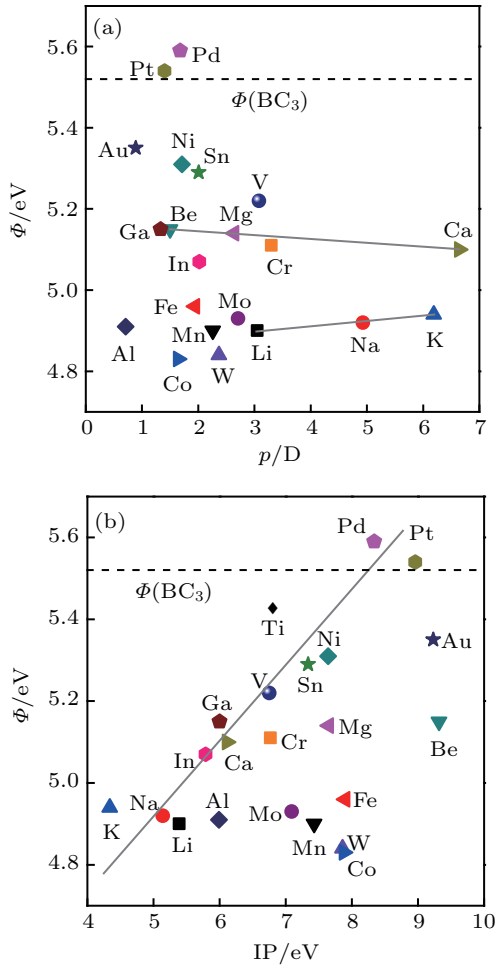


Fig. 8. (color online) (a) The dipole moments p vs. the work functions Φ and (b) the IP vs. the work function Φ for all adatoms adsorbing on their most stable sites.

4. Conclusion

In summary, we have studied the adsorption properties of alkali, alkaline-earth, groups III–IV, and transition metals on the graphene-like BC_3 sheet. Many interesting properties are concluded. (1) The interactions between the adatoms and the BC_3 are quite strong in contrast to those found in adatoms-graphene. (2) For Li, Na, and K on BC_3, the adatom s states lie far above from E_F, which results in the ionic bond for these adatoms. For Be, Mg, and Ca adatoms, besides the ionic bonding, there exist hybridizations between adatoms and the substrate near E_F. The Al, Ga, In, and Sn adatoms are covalently bounded with the nearest neighboring atoms of the BC_3 sheet. The adatom d states of all transition metal atoms studied are strongly hybridized with the BC_3 states around E_F except for Au, whose s states are hybridized with the substrate near E_F. (3) BC_3 with Co adatom reveals a quantum anomalous Hall (QAH) insulator phase as inferred from LDA calculations. (4) For Mo and Mn adatoms on BC_3, the structures exhibit half metal behavior, while the most stable Au–BC_3 structure is spin-semiconductor. (5) For Li, Na, K, Ca, Ga, In, Sn, Ti, V, Cr, Ni, Pd, and Pt, there is a trend that adatom species with lower IP have lower Φ. These results indicate the potential applications of the functionalization of graphene-like BC_3 with metal adatoms.

References

[1] Novoselov K S, Geim A K, Morozov S V, Jiang D, Zhang Y, Dubonos S V, Grigorieva I V and Firsov A A 2004 *Science* **306** 666
[2] Katsnelson M I, Novoselov K S and Geim A K 2006 *Nat. Phys.* **2** 620
[3] Novoselov K S, Geim A K, Morozov S V, Jiang D, Katsnelson M I, Grigorieva I V, Dubonos S V and Firsov A A 2005 *Nature* **438** 197
[4] Berger C, Song Z, Li T, Li X, Ogbazghi A Y, Feng R, Dai Z, Marchenkov A N, Conrad E H, First P N and de Heer W A 2006 *Science* **312** 1191
[5] Zhang Y, Tan W Y, Stormer H L and Kim P 2005 *Nature* **438** 201
[6] Elias D C, Nair R R, Mohiuddin T M G, Morozov S V, Blake P, Halsall M P, Ferrari A C, Boukhvalov D W, Katsnelson M I, Geim A K and Novoselov K S 2009 *Science* **323** 610
[7] Sofo J O, Chaudhari A S and Barber G D 2007 *Phys. Rev. B* **75** 153401
[8] Sahin H, Ataca C and Ciraci S 2009 *Appl. Phys. Lett.* **95** 222510
[9] Sahin H, Ataca C and Ciraci S 2010 *Phys. Rev. B* **81** 205417
[10] Topsakal M, Cahangirov S and Ciraci S 2010 *Appl. Phys. Lett.* **96** 091912
[11] Dikin D A, Stankovich S, Zimney E J, Piner R D, Dommett G H B, Evmenenko G, Nguyen S T and Ruoff R S 2007 *Nature* **448** 457
[12] Eda G, Fanchini G and Chhowalla M 2008 *Nat. Nanotechnol.* **3** 270
[13] Robinson J T, Perkins F K, Snow E S, Wei Z and Sheehan P E 2008 *Nano Lett.* **8** 3137
[14] Nair R R, RenW, Jalil R, Riaz I, Kravets V G, Britnell L, Blake P, Schedin F, Mayorov A S, Yuan S, KatsnelsonMI, Cheng H M, StrupinskiW, Bulusheva L G, Okotrub A V, Grigorieva I V, Grigorenko A N, Novoselov K S and Geim A K 2010 *Small* **6** 2877
[15] Robinson J T, Burgess J S, Junkermeier C E, Badescu S C, Reinecke T L, Perkins F K, Zalalutdniov M K, Baldwin J W, Culbertson J C, Sheehan P E and Snow E S 2010 *Nano Lett.* **10** 3001
[16] Withers F, Dubois M and Savchenko A K 2010 *Phys. Rev. B* **82** 073403
[17] Leenaerts O, Peelaers H, Hernandez-Nieves A D, Partoens B and Peeters F M 2010 *Phys. Rev. B* **82** 195436
[18] Sahin H, Topsakal M and Ciraci S 2011 *Phys. Rev. B* **83** 115432
[19] Chan K T, Neaton J B and Cohen M L 2008 *Phys. Rev. B* **77** 235430
[20] Ataca C, Aktürk E, Ciraci S and Ustunel H 2008 *Appl. Phys. Lett.* **93** 043123
[21] Ataca C, Aktürk E and Ciraci S 2009 *Phys. Rev. B* **79** 041406(R)
[22] Ao Z M and Peeters F M 2010 *Phys. Rev. B* **81** 205406
[23] Profeta G, Calandra M and Mauri F 2012 *Nat. Phys.* **8** 131
[24] Zhang H, Lazo C, Blügel S, Heinze S and Mokrousov Y 2012 *Phys. Rev. Lett.* **108** 056802
[25] Cao C, Wu M, Jiang J and Cheng H P 2010 *Phys. Rev. B* **81** 205424
[26] Ü. Aktürk O and Tomak M 2009 *Phys. Rev. B* **80** 085417
[27] Krasheninnikov A V, Lehtinen P O, Foster A S, Pyykkö P and Nieminen R M 2009 *Phys. Rev. Lett.* **102** 126807
[28] Rodríguez-Manzo J A, Cretu O and Banhart F 2010 *ACS Nano* **4** 3422

[29] Beheshti E, Nojeh A and Servati P 2011 *Carbon* **49** 1561
[30] Liu C and Zeng Z 2010 *Appl. Phys. Lett.* **96** 123101
[31] Kim G, Jhi S, Lim S and Park N 2009 *Phys. Rev. B* **79** 155437
[32] Liu J, Wu J, Chen C, Han L, Zhu Z and Wu J 2017 *Int. J. Mod. Phys. B* **32** 1850033
[33] Yanagisawa H, Tanaka T, Ishida Y, Matsue M, Rokuta E, Otani S and Oshima C 2004 *Phys. Rev. Lett.* **93** 177003
[34] Tanaka H, Kawamata Y, Simizu H, Fujita T, Yanagisawa H, Otani S and Oshima C 2005 *Solid State Commun.* **136** 22
[35] Yang Z and Ni J 2012 *Appl. Phys. Lett.* **100** 183109
[36] Zhao Y, Dai Z, Sui P and Wang W 2014 *J. Phys. Chem. Solids* **75** 1137
[37] Chen X and Ni J 2013 *Phys. Rev. B* **88** 115430
[38] Chen X, Yao Y, Yao H, Yang F and Ni J 2015 *Phys. Rev. B* **92** 174503
[39] Lin X and Ni J 2012 *Phys. Rev. B* **86** 075440
[40] Sahin H and Peeters F M 2013 *Phys. Rev. B* **87** 085423
[41] Kresse G and Hafner J 1993 *Phys. Rev. B* **47** 558
[42] Kresse G and Joubert D 1999 *Phys. Rev. B* **59** 1758
[43] Perdew J P, Burke K and Ernzerhof M 1996 *Phys. Rev. Lett.* **77** 3865
[44] Monkhorst H J and Pack J D 1976 *Phys. Rev. B* **13** 5188
[45] Makov G and Payne M C 1995 *Phys. Rev. B* **51** 4014
[46] Neugebauer J and Scheffler M 1992 *Phys. Rev. B* **46** 16067
[47] Miyamoto Y, Rubio A, Louie S G and Cohen M L 1994 *Phys. Rev. B* **50** 18360
[48] Yanagisawa H, Tanaka T, Ishida Y, Matsue M, Rokuta E, Otani S and Oshima C 2004 *Phys. Rev. Lett.* **93** 177003
[49] Mills G, Jónsson H and Schenter G K 1995 *Surf. Sci.* **324** 305
[50] Kittel C 2005 *Introduction to Solid Sate Physics* (8th edn.) (New York: Wiley)
[51] Martin W C and Wiese W L 1996 *Atomic, Molecular, and Optical Physics Handbook*, editor Drake G W F (New York: American Institute of Physics) pp. 135–153
[52] Yu R, Zhang W, Zhang H J, Zhang S C, Dai X and Fang Z 2010 *Science* **329** 61
[53] Jin H, Im J and Freeman A J 2011 *Phys. Rev. B* **84** 134408
[54] Son Y, Cohen M L and Louie S G 2006 *Nature* **444** 347
[55] Wang X L 2008 *Phys. Rev. Lett.* **100** 156404
[56] Zhao Y and Ni J 2014 *Phys. Chem. Chem. Phys.* **16** 15477
[57] Weng H M, Dai X and Fang Z 2014 *Progress in Physics* **34** 1
[58] Ding J, Qiao Z, Feng W, Yao Y and Niu Q 2011 *Phys. Rev. B* **84** 195444
[59] Zhang H, Lazo C, Blügel S, Heinze S and Mokrousov Y 2012 *Phys. Rev. Lett.* **108** 056802